

MAGNETIC DOMAINS IN HEMATITE

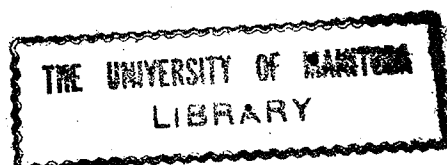
A thesis

Submitted to

The Faculty of Graduate Studies, University of
Manitoba, in partial fulfillment of the
requirements of the degree of Doctor of Philosophy.

By

John A. Eaton,
Winnipeg, Manitoba,
May, 1970.



Abstract

The aim of the research in this thesis was to determine by all means available the magnetic domain structure of synthetic single crystal hematite and any other related properties. The magnetic domain structure was determined by the magnetite colloid technique. Ideally, it was 180° slab-type structure with the walls parallel to the basal plane. Magnetoelastic interactions with strain causing crystal defects produced distortions from this in the bulk crystal structure to maze-like or cylindrical 180° domains with parallel axes in the basal plane which changed direction if magnetoelastic interactions demanded it. In thin sections, the magnetoelastic effect caused the appearance of a two phase domain structure of $2\phi < 180^\circ$ walls where ϕ varied. The plane of these walls was parallel to basal plane easy direction and at $\sim 26^\circ$ to the basal plane. A 180° structure could disappear abruptly or more generally by these 2ϕ walls. Magnetoelastic interactions with regular lattice distortions caused by the growth structure appeared to stabilize a narrow strip domain pattern of 2ϕ walls in bulk (110) surfaces.

The magnetic domain observations also allowed the

Morin transition process to be observed. A colloid wall formed at the boundary between the antiferromagnetic-weakly ferromagnetic phases. The transition always occurred by a process of adjacent (110) growth layers going through the transition in succession as temperature varied. The transition temperature range was consistent with bulk measurements and was found to be caused by a non-uniform doping which also followed the growth structure. The shift was also related to difference of dopant ionic size from the Fe ionic size. Domain behaviour in this process appeared to be nothing more than a response to a changing boundary of the ferromagnetic phase. The domain structure generally showed a little or no changes in the process.

Mössbauer, magnetometer and crystal physical property measurements gave further support to the models proposed for the domain and transition behaviour.

Wall models consistent with magnetoelastic anisotropy were developed which explained the domain walls. Domain wall energies were calculated to be $\sim 4-13 \times 10^{-2}$ ergs/cm² which agreed with domain observations.

Acknowledgements

The author wishes to thank Professor A. H. Morrish for his support and encouragement that made this research possible. Also, the invaluable discussions with Professor C. W. Searle and his advice are very much appreciated. He would also like to thank many of his fellow graduate students for their cooperation and help. Finally, he would like to thank his family especially his wife, Phyllis, without whom this thesis would not have been possible.

Table of Contents

Abstract	
Acknowledgements	
I. Introduction	1
II. Preliminary Considerations	3
A. The Magnetic Free Energy	3
B. Principles of Domain Formation	14
C. Principles of the Bitter Figure Technique	24
III. Experimental Technique	28
A. Crystals and Their Preparation	28
B. Preparation of the Magnetite Colloid	33
C. Magnetite Colloid Domain Observations	34
1. At Room Temperature	34
2. Between -40°C and 50°C	36
D. Crystal Physical Properties	39
1. X-ray Diffraction	39
2. X-ray Fluorescence	40
3. Electron Microprobe Analysis	40
4. X-ray Topographic and Optical Studies	41

E.	Bulk Magnetization Properties	44
1.	Magnetometer Measurements	44
2.	Mössbauer Spectrometer Measurements	46
IV.	Experimental Results	49
A.	Magnetite Colloid Domain Patterns	49
1.	At Room Temperature	49
a)	No Magnetic Field or Stress	49
b)	With Applied Magnetic Field	55
c)	With Applied Stress and Magnetic Fields	65
2.	Colloidal Structures at the Morin Transition	68
B.	Crystal Physical Properties	80
1.	X-ray Diffraction and X-ray Fluorescence	80
2.	Electron Microprobe Analysis	83
3.	X-ray Topographic and Optical Observations	88
C.	Bulk Magnetization Measurements	91
1.	Magnetometer Measurements	91
2.	Mössbauer Spectra Observations	96

V. Discussion of Results	103
A. The Domain Structure of Hematite	103
1. The Orientation of the Domains'	
Magnetizations	103
2. The Structure of the Domain Walls	112
a) The N-Domain Wall	112
b) The C- and CN-Domain Walls	117
B. The Morin Transition	120
C. Bulk Magnetization Measurements	124
1. Magnetometer Measurements	124
2. Mössbauer Measurements	126
D. Crystal Physical Characteristics	127
VI. Conclusions	129
A. The Domain Structure	129
B. The Morin Transition	129
C. The Physical Characteristics of	
Hematite Crystals	130
D. Suggestions for Further Experiments	130

References

Tables

I. Domain magnetostatic and wall energies	23
II. Mechanical polishing procedure	29
III. Width of domains	56
IV. Average Distortion of Hematite Lattice from $F_e K\alpha_1$ (232) and (318) Reflections	81
V. Mössbauer Spectra Parameters for (1 $\bar{1}$ 0) Thin Section	99

Figures

1. Rhombohedral unit cell of hematite and coordinate system to which spins are referred	5
2. Domain configurations for energy formula of Table I	22
3. Fringing field models for domain walls at crystal surface	26
4. Laue photographs of $(1\bar{1}0)$ and $(11\bar{2})$ planes	30
5. Geometry of $(1\bar{1}0)$ and $(11\bar{2})$ planes relative (110) planes	31
6. Stress apparatus	37
7. Temperature control apparatus	38
8. X-ray topography camera	42
9. Mössbauer experiment geometry for spin axis direction determination	47
10. N-domain patterns	50
11. C- and CN-domain patterns	52
12. Effect of magnetic field, in basal plane, parallel and perpendicular to a $(11\bar{2})$ thin section having N-domains	57
13. Effects of defect on magnetic field behaviour in a $(11\bar{2})$ thin section	59

14.	Magnetic field behaviour of CN-domains and unusual effects related to CN-domains	62
15.	Graph of magnetization versus field according to domain widths in $(1\bar{1}0)$ and $(11\bar{2})$ thin sections	64
16.	Graph of N-domain width for a $(1\bar{1}0)$ thin section versus applied stress	66
17.	The Morin transition for (110) surface of pure bulk crystal	69
18.	The Morin transition in pure 2 mole % Ga doped thin section	70
19.	The Morin transition in Ti doped bulk and thin section (110) surfaces	71
20.	The WF-AF phase boundaries as a function of temperature on 0.5 mole % Rh doped bulk crystal surface	75
21.	The WF-AF phase boundaries on a 1.0 mole % Rh doped crystal	76
22.	The WF-AF phase boundaries on a 0.1 mole % Ti doped crystal	77
23.	Photographs of crystal surfaces showing scan paths for electron microprobe analysis	82
24.	Graph of T_M versus doping for 0.5 mole % Rh doped surface	84

25.	Graph of T_M versus doping for 1.0 mole % Rh doped crystal	85
26.	Graph of T_M versus doping for 0.1 mole % Ti doped crystal	86
27.	Graph of doping along scan paths for 0.5 mole % Ga and 1.0 mole % Al doped crystals	87
28.	Photographs of crystals and crystal surfaces	89
29.	Hysteresis loops of a poor quality large bulk crystal before and after a 1200°C anneal	92
30.	Hysteresis loops of a good quality bulk crystal before and after 1200°C anneal	93
31.	Hysteresis loop of small bulk crystal	94
32.	Magnetization versus field up to saturation for small bulk crystal	95
33.	Magnetization as versus temperature at 100 Oe and 15 kOe for 0.5 mole % Rh doped crystal	97
34.	Magnetization versus temperature at 100 Oe for 1.0 mole % Rh doped crystal	98
35.	Mössbauer spectra for $\pm 15^\circ$ and 0° orientations of a $(1\bar{1}0)$ thin section	102
36.	Model for an AF-F domain wall parallel to the basal plane	113
37.	Model for a F wall parallel to the basal plane	114

I. Introduction

Hematite, or $\alpha\text{-Fe}_2\text{O}_3$, which is readily obtainable in large single crystals from nature, has a very weak magnetization at room temperature. Thus, in the past considerable research, has been devoted to the magnetic properties of hematite. This was, no doubt, stimulated by the research of Morin¹ and of Shull et al². In 1950, Morin observed that hematite underwent a transition, now called the Morin transition, where the susceptibility rapidly increased with temperature. The Morin transition temperature T_M has now been measured to be $T_M \sim -10$ C for very pure synthetic single crystal hematite. Then in 1951, Shull et al determined that hematite existed in what appeared to be two different antiferromagnetic states above and below the transition. In the next few years various researchers attempted to explain the weak moment in terms of crystal defects, impurities and even a net moment generated in antiferromagnetic domain walls. Finally, Dzialoshinskii³ produced the now accepted thermodynamic argument which showed that in the one antiferromagnetic state it was possible for the sublattice spins to be slightly canted towards each other without lowering the magnetic symmetry. The quantum mechanical basis of this canting was subsequently given by Moriya⁴ as a spin-orbit effect in the super-exchange interaction. Continued interest in hematite up to the present time has mainly been concerned

with measurement and explanation of effects related to magnetocrystalline anisotropy and magnetostriction.

Since hematite has an ordered ferromagnetic component, although very weak, a domain structure could be expected to exist. This was indeed shown to be the case by Blackman et al⁵ and William et al⁶ and has now been well established by the continued work by various researchers⁷⁻¹¹ under M. Blackman. Also, it has been established that the domain structure disappears in a characteristic fashion at the Morin transition.

Since we have a supply of, and could grow, large highly perfect,¹² pure and doped, crystals of hematite by a method established by P.J. Besser¹³ it was felt that we might be able to contribute towards further explanation of the domain structure of hematite. Therefore, it is the purpose of this thesis, to put forward all the results of a research program into the domain structure in hematite.

II. Preliminary Considerations

A. The Magnetic Free Energy

Domain structures in ferromagnetic materials are a mechanism by which the magnetic free energy can be minimized. Therefore, to explain domain structures a knowledge of the mechanisms that can contribute to the magnetic free energy is necessary. The magnetic free energy can be expressed¹⁴

$$F_T = F_H + F_D + F_e + F_K + F_\sigma + F_o \quad (1)$$

where F_H is the free energy due to an applied magnetic field, F_D the self energy due to uncompensated poles, F_K the magnetocrystalline anisotropy energy, F_σ the magnetostrictive energy, F_e the exchange energy and F_o the energy due to any other magnetic interactions relevant to the material such as crystalline imperfections. Thus, this expression is completely general and can be applied to any magnetically ordered material if the form of all the magnetic interactions is known.

The energy due to an applied field \underline{H} is

$$F_H = - \int \underline{m} \cdot \underline{H} dv \quad (2)$$

and the self magnetostatic energy is

$$F_D = -\frac{1}{2} \int \underline{m} \cdot \underline{H}_D dv \quad (3)$$

where \underline{m} is the magnetization and \underline{H}_D is the self field due to uncompensated poles. For a uniformly magnetized ellipsoid

$$F_D = \frac{1}{2} D m^2 \quad (4)$$

where D is a geometrical factor depending on the shape of the ellipsoid relative to the direction of magnetization

and is relatively easy to calculate.¹⁴ However, calculation of demagnetization energies for other than ellipsoid shaped specimens becomes very complicated and laborious and usually involves approximations.

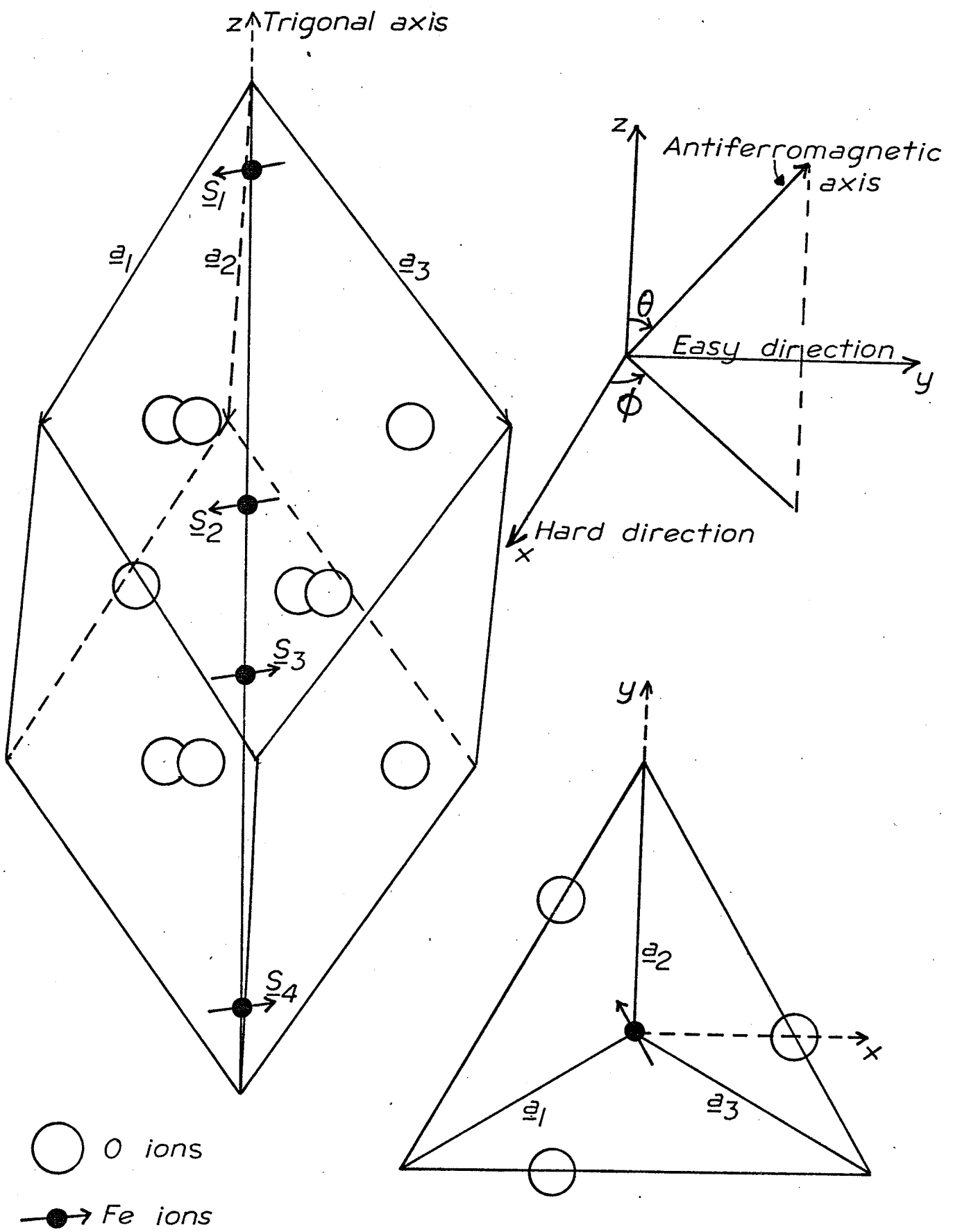
The remainder of the terms in equation (1), ignoring F_0 , generally depend on crystal and magnetic symmetry. Therefore, a discussion of the crystal structure of hematite is appropriate at this point.

Hematite has a trigonal structure with space group $R\bar{3}c$ as determined by Pauling et al.¹⁵ and later refined by Blake et al.¹⁶ The structure can be represented either by a rhombohedral or a hexagonal lattice. The rhombohedral cell is illustrated in Fig. 1. The structure may be described as a slightly distorted hexagonal close packed structure of oxygen atoms with $2/3$ of the octahedral interstices containing iron atoms. The iron atoms are so arranged such that, along any hexagonal axis, every third interstice is empty. Therefore, the lattice repeats itself after every six layers of oxygen atoms.

The microscopic origin of ordering in magnetic systems is the exchange interaction.¹⁷ This interaction arises between neighbouring magnetic ions because of the effect of the Pauli Exclusion Principle and the indistinguishability of electrons when the outermost electron orbitals of the two ions overlap. This generally results in the ions having

Figure 1.

Rhombohedral unit cell of hematite. The relative direction of the spins and the coordinate system to which they will always be referred are indicated on the unit cell.



parallel spin configurations as the lowest energy state. This interaction energy between the spins of the ions summed over the whole crystal can be represented, assuming only nearest neighbour interactions and isotropy of the exchange interaction as

$$F_e = -2J_e \sum \underline{S}_i \cdot \underline{S}_j \quad (5)$$

$J_e > 0$ is the exchange integral and \underline{S}_i the sum of the unpaired spins on the ion.

The exchange interaction may also occur via an intermediate non-magnetic ion such as oxygen as in the case of hematite. This interaction is now called superexchange and the quantum mechanical formalism has been developed by Anderson¹⁷. For cases where superexchange is appreciable the direct exchange is negligible since the magnetic ions are too widely separated. Therefore, in hematite, appreciable overlap occurs between the p electron states of the O^{2-} ion and the outer d electron states of the Fe^{+++} ion. In the O^{2-} ground state the two p electrons are antiparallel. Therefore, if the d electron states on two magnetic ions have appreciable overlap with the same O^{2-} ion, the spins have an antiparallel configuration as the lowest energy state. Since the p state is dumbbell shaped this interaction is appreciable only if the Fe-O-Fe bond are appreciably different from 90° . According to Gilleo¹⁸, for each Fe ion, there are nine appreciable interactions in hematite. Thus, the magnetic moments of the iron ions are orientated

in two antiparallel sublattices formed by alternate layers of ions parallel to the basal plane ((111) plane in rhombohedral representation).

Phenomenologically this interaction may be represented in the molecular field approximation¹⁴ by

$$\lambda \underline{M}_1 \cdot \underline{M}_2 \quad (6)$$

where \underline{M}_1 and \underline{M}_2 are the sublattice magnetizations and λ is the exchange constant. Then $\lambda \underline{M}_1$ represents the molecular field of one sublattice acting on the other. There is no evidence to suggest that there is anything but a negligible exchange interaction between spins of the same sublattice.

In some basically antiferromagnetic materials with sufficiently low symmetry, such as hematite, Dzialoshinskii showed by a thermodynamic argument that it was possible for the sublattices to cant towards each other without lowering the symmetry of the magnetic state. If the thermodynamic potential of a magnetic state is expanded in terms of spin variables, then under the magnetic symmetry group for the antiferromagnetic axis in the basal plane, terms of the form

$$l_x m_y - l_y m_x \quad (7)$$

are allowed. The vector $\underline{l} = (l_x, l_y, l_z) = \underline{S}_1 + \underline{S}_2 - \underline{S}_3 - \underline{S}_4$ defines the antiferromagnetic spin axis and the vector $\underline{m} = (m_x, m_y, m_z) = \underline{S}_1 + \underline{S}_2 + \underline{S}_3 + \underline{S}_4$ is the net magnetic moment. The spin vectors \underline{S}_i and the cartesian coordinate system to which all calculations will be referred are illustrated

on the rhombohedral unit cell in Fig. 1. The interaction can be expressed in the molecular field approximation by

$$\underline{D} \cdot (\underline{M}_1 \times \underline{M}_2) \quad (8)$$

where \underline{D} is the Dzialoshinskii canting vector parallel to the $[111]$ axis.

The microscopic origin of this interaction was formulated by Moriya⁴ who extended the formalism of Anderson¹⁷ to include spin-orbit effects in the superexchange interaction. This leads to an anisotropic term whose form is exactly similar to that of the molecular field approximation. Thus, the total exchange energy in hematite can be expressed, for the antiferromagnetic axis in the basal plane, as

$$F_e = \lambda \underline{M}_1 \cdot \underline{M}_2 + \underline{D} \cdot (\underline{M}_1 \times \underline{M}_2) = \lambda M^2 \cos 2\theta + \mathcal{D} M^2 \sin 2\theta \quad (9)$$

where θ is the canting angle and $|\underline{M}_1| = |\underline{M}_2| = M$ is the sublattice magnetization. Minimizing F_e with respect to θ gives the canting angle as

$$\theta_D = \frac{\mathcal{D} M}{2 \lambda M} = \frac{H_D}{2H_e} \quad (10)$$

where H_e is the exchange field and H_D is the canting field.

For pure hematite, resonance experiments^{19,20} give values of $\mathcal{D} M \sim 2.2 \times 10^4$ Oe and from susceptibility measurements^{21,22}

$\lambda M \sim 10^7$ Oe. Thus, the canting angle is $\theta_D \sim 1.1 \times 10^{-3}$

radians. The spontaneous moment $m = 2M \theta_D$, from static measurements^{23,24} has values ~ 2.0 emu/cc. A value of $M = 880$ emu/cc obtained by Mössbauer technique,²⁴ gives a value of m

~ 2.1 emu/cc which agrees with the static measurements.

Phenomenologically, the magnetocrystalline anisotropy energy F_K can be expressed²⁰ as

$$F_K = K_1 \sin^2 \theta + K_2 \sin^4 \theta + K_3' \sin^6 \theta + K_3 \sin^6 \theta \cos 6\phi \quad (11)$$

where θ is the angle the antiferromagnetic axis makes with the z axis and ϕ is the angle the projection of the antiferromagnetic axis in the x-y plane makes with the x axis. The first three terms are the uniaxial components and the last term is the three fold basal plane anisotropy. Microscopic origins for these anisotropies come from two main sources^{25,26}; the magnetic dipolar anisotropy and the single ion anisotropy due to spin-orbit effects. Neglecting the contributions to the 3 fold basal plane anisotropy the contribution of the magnetic dipolar anisotropy was calculated to have an effective field value $H_{MD} \sim -10^4$ oe at absolute zero which favours the antiferromagnetic axis parallel to the trigonal axis. However, the uniaxial contribution from the single ion anisotropy favours the basal plane orientation of the antiferromagnetic axis. It is the competition between these two anisotropies which produce the Morin transition. Thus, at the Morin transition the effective field value of the uniaxial part of the single ion anisotropy $H_{SI} = -H_{MD}$ and therefore, in the neighbourhood of the transition $H_{SI} \sim |H_{MD}|$. The effective uniaxial anisotropy field above is

then $H_{SI} - |H_{MD}|$. From spin flop data²⁰ $H_{K_1} = H_{SI} - |H_{MD}| = 217$ Oe at 0°K. Therefore, in the temperature range of interest between the Morin transition and room temperature, $0 < H_{K_1} < \sim 1000$ Oe gives a value for $K_1 = MH_{K_1}$ in the range 0 to 10^6 ergs/cm³.

The basal plane anisotropy field has been measured by microwave resonance^{20,27} to have an effective field value ~ 1.1 to 1.8×10^{-2} Oe. Therefore, the value of $K_3 = \frac{MH_{K_3}}{18}$ is ~ 0.5 to 1.0 ergs/cm³.

In general every magnetic state induced or spontaneous is accompanied by an anisotropic deformation of the crystal called magnetostriction. This deformation will exhibit the same symmetry as the crystal space group. Linear magnetostriction is the deformation induced by an applied magnetic field. In hematite, it was observed and measured by Anderson et al²⁸ for the purely antiferromagnetic state in hematite. Piezomagnetism, the inverse of linear magnetostriction has been discussed and also observed by various researchers.²⁹ However, the effect that is important to the domain properties is the spontaneous magnetostriction associated with the direction of the antiferromagnetic axis. The spontaneous magnetostriction can be found by minimizing the sum of the elastic energy and the magnetoelastic energy. The resulting equilibrium strain deformation is the spontaneous magneto-

striction. The elastic and magnetoelastic coupling coefficients are fourth order polar tensors and the energies associated with them are^{27,30} respectively

$$\begin{aligned}
 E_e = & \frac{1}{2}C_{11}e_{xx}^2 + C_{12}e_{xx}e_{yy} + C_{13}e_{xx}e_{zz} + 2C_{14}e_{xx}e_{yz} & (12) \\
 & + \frac{1}{2}C_{11}e_{yy}^2 + C_{13}e_{yy}e_{zz} - 2C_{14}e_{yy}e_{yz} \\
 & + \frac{1}{2}C_{zz}e_{zz}^2 \\
 & + 2C_{44}e_{yz}^2 \\
 & + 2C_{44}e_{xz}^2 + 2C_{14}e_{xz}e_{yz} \\
 & + (C_{11} - C_{12})e_{xy}^2
 \end{aligned}$$

and

$$\begin{aligned}
 E_{me} = & B_{11}\gamma_x^2e_{xx} + B_{12}\gamma_x^2e_{yy} & + B_{14}\gamma_x^2e_{yz} & (13) \\
 & B_{12}\gamma_y^2e_{xx} + B_{11}\gamma_y^2e_{yy} & - B_{14}\gamma_y^2e_{yz} \\
 & + B_{zz}\gamma_z^2e_{zz} \\
 & B_{41}\gamma_y\gamma_z e_{xx} - B_{41}\gamma_y\gamma_z e_{yy} & + B_{44}\gamma_y\gamma_z e_{yz} \\
 & + B_{44}\gamma_x\gamma_z e_{xz} + 2B_{41}\gamma_x\gamma_z e_{xy} \\
 & + 2B_{14}\gamma_x\gamma_y e_{xz} + 2(B_{11} - B_{12})\gamma_x\gamma_y e_{xy}
 \end{aligned}$$

where C_{ij} , B_{ij} , e_{ij} and γ_i are the elastic constants, the magnetoelastic coupling constants, the strains and the direction cosines of the antiferromagnetic axis respectively.

Then by forming $\frac{\partial}{\partial e_{ij}} (E_e + E_{me}) = 0$, a set of equations is

obtained from which the equilibrium strains can be found.

Assuming the spin axis is constrained to the basal plane

then the solutions to the equilibrium strains²⁷, after

correcting them³⁰ to give the exact solution, are:

$$e_{xx} = \frac{C_{33}(B_{11} + B_{12}) + 2C_{13}B_{33}}{2 \left[C_{33}(C_{11} + C_{12}) - 2C_{13}^2 \right]} + \frac{[C_{14}B_{14} - C_{44}(B_{11} - B_{12})]}{2 \left[C_{44}(C_{11} - C_{12}) - 2C_{14}^2 \right]} \cos 2\phi$$

$$= M + N \cos 2\phi$$

$$e_{yy} = M - N \cos 2\phi \quad (14)$$

$$e_{zz} = \frac{C_{13}(B_{11} + B_{12}) + (C_{11} + C_{12})B_{33}}{C_{33}(C_{11} + C_{12}) - 2C_{13}^2} = K$$

$$e_{xy} = N \sin 2\phi$$

$$e_{xz} = \frac{[2C_{14}(B_{11} - B_{12}) - (C_{11} - C_{12})B_{14}]}{4 \left[C_{44}(C_{11} - C_{12}) - 2C_{14}^2 \right]} \sin 2\phi = L \sin 2\phi$$

$$e_{yz} = L \cos 2\phi$$

Physically this deformation can be interpreted²⁷ as consisting of three parts: firstly, a uniform deformation independent of the antiferromagnetic axis direction, secondly, a